中國機械工程學刊第四十三卷第二期第 117~125 頁(民國一百一十一年)
Journal of the Chinese Society of Mechanical Engineers, Vol.43, No.2, pp117~125 (2022)

Improvement on the Efficiency of AMR Refrigeration Systems with Staggered Laminated Plates

Che-Wei Chang and Wen-Jenn Sheu*

ABSTRACT

Refrigeration of active magnetic regenerator (AMR) with no refrigerant consumption and compressors is a promising refrigeration technology. From a viewpoint of heat transfer, two problems restrict the efficiency of AMR. Weak heat transfer between magnetocaloric material (MCM) and working fluid as well as conducted heat from hot to cold side decreases the refrigeration capacity. To improve the two weaknesses, staggered breaking segments in rectangular MCM plates are adopted. AMR models with a length of 80 mm are analyzed numerically. As compared to the model with no breaking segments, the model C1 can reduce mass usage of MCM by 2.5%, increase the cooling power from 62.48 to 69.10 watts with the magnetic field of 0-1 T, the temperature span of 283-303 K, the operation period of 0.6 seconds, and the utilization factor of about 0.4. This study shows that the performance of novel AMR can be improved with staggered laminated plates.

Keywords: active magnetic regenerator (AMR), magnetocaloric material (MCM), staggered breaking segments.

NOMENCLATURE

Symbols

a_s	Area between solid and liquid (m^2)
c_P	Specific heat at constant pressure ($J\ kg^{-1}\ K^{-1}$)
D_h	Hydraulic diameter (m)
Gz	Graetz number
h	Convective heat transfer coefficient ($W\ m^{-2}\ K^{-1}$)
$H_{channel}$	Distance between two parallel plates (m)
H_{plate}	Thickness of a MCM plate (m)
k	Thermal conductivity ($W\ m^{-1}\ K^{-1}$)
L	Length of AMR (m)
m	Mass (kg)
$\dot{m}$	Mass flow rate ($kg\ s^{-1}$)
N	Number of breaking segments in a level of a MCM plate
Nu	Nusselt number
p	Pressure (Pa)
P	Period of an AMR cycle
p_{gage}	Gage pressure (Pa)
Pr	Prandtl number
$\dot{q}_c$	Specific cooling power based on AMR weight in an cycle ($W\ kg^{-1}$)
$\dot{q}_h$	Specific heating power based on AMR weight in an cycle ($W\ kg^{-1}$)
$\dot{q}_{MCE}$	Equivalent heating power of magnetocaloric effect ($W\ m^{-3}$)
$\dot{Q}_c$	Cooling power in an AMR cycle (W)
$\dot{Q}_h$	Heating power in an AMR cycle (W)
Re	Reynolds number
t	Time (s)
t_{blow}	$t_{blow} = t_2 = t_4$
t_{MCE}	Magnetizing/demagnetizing time in an AMR cycle (s)
t_1	Flow-stagnation time before hot blows in an AMR cycle (s)
t_2	Hot blow time in an AMR cycle (s)
t_3	Flow-stagnation time before cold blows in an AMR cycle (s)
t_4	Cold blow time in an AMR cycle (s)
T	Temperature (K)
T_H	Hot-side temperature of AMR (K)
T_L	Cold-side temperature of AMR (K)
u, v, w	Velocity components in the (*x, y, z*) system of coordinates ($m\ s^{-1}$)
$\bar{V}$	Average velocity ($m\ s^{-1}$)
x, y, z	Cartesian coordinates

Greek Symbols

ΔT_{ad}	Adiabatic temperature change (K)
μ	Viscosity coefficient ($kg\ m^{-1}\ s^{-1}$)

Paper Received August, 2021. Revised January, 2022. Accepted January, 2022. Author for Correspondence: Wen-Jenn Sheu.

* *Professor, Department of Power Mechanical Engineering, National Tsinghua University, Hsinchu, 30013, Taiwan, R.O.C.*

* *Corresponding author. Tel: +886 3 574 2099
E-mail: wjsheu@mx.nthu.edu.tw*

ρ	Density (kg m^{-3})
φ	Utilization factor

Subscripts

$(\ )_f$	Fluid
$(\ )_{i,k}$	Dimensions in space
$(\ )_{MCE}$	MCM
$(\ )_{MCM}$	MCM

Abbreviations

AMR	Active magnetic regenerator
MCE	Magnetocaloric effect
MCM	Magnetocaloric material
MFT	Mean field theory

INTRODUCTION

The refrigeration system of active magnetic regenerator (AMR) cycle is a promising technology to lower the cost of refrigeration usage. The 20-30% energy is consumed in a variety of refrigeration systems in the world. It is estimated that the approximately 15% amount of energy usage could be reduced by using AMR system (Gschneidner and Pecharsky, 2008). A pump with solid-state magnetocaloric material (MCM) instead of a high-pressure compressor in traditional refrigeration systems is adopted for refrigeration systems of AMR. The refrigerant which is not environmentally friendly is not needed. However, many complicated problems exist in AMR. The operation period is limited by a small rate of convective heat transfer between solid MCMs and working fluid. The conductive heat transfer through solid MCM from hot to cold end in an axial direction lowers the performance of AMR. The investigation of temperature distribution in AMR for varied system parameters is difficult to be studied experimentally due to thin MCM sheets and fluid channels of AMR apparatuses and less studied two or three dimensional numerical models.

To achieve a greater temperature span and use some MCM alloys with no rare-earth elements (Franco et al., (2012), many current AMR apparatuses employed multi-layered magnetic regenerators composed of MCM with different Curie points (Mahdy, 2017). To develop MCM with different Curie temperature and reduce the usage of rare-earth elements became a major research interest (Liu et al., 2012; Shah et al., 2017; Yu et al., 2003; Balli et al., 2007; Chen et al., 2003; Balli et al., 2017; Gschneidner et al., 2005). However, the magnets based on neodymium ($Nd_2Fe_{14}B$) used in most of AMR cooling systems also contain rare-earth-material (Klinar et al., 2019). The AMR magnet designs of C-shaped magnets (Tušek et al., 2009), Halbach Arrays (Raich and Blümler, 2004), and C-shape magnet formed by Halbach array (Lee et al., 2002) were studied to intensify a magnetic field. Moreover, a magnet assembly for AMR Carnot cycle instead of a Brayton one was investigated by Kitanovski et al. (2014).

Recently, researches of matching the main parameters of near room-temperature AMR prototypes have been focused on. Mechanically, not only linear relative motion devices but also rotational ones were built. Reviews of AMR test devices were reported in (Gschneidner and Pecharsky, 2008; Yu et al., 2010). Most of them functioned with AMR cycle consist of four basic steps: magnetization, magnetic field increasing at adiabatic process and temperature of MCM growing due to MCE; hot blow, fluid flowing from cold side to hot one at isomagnetic process, absorbing heat from MCM, and discharging heat to the heat exchanger at hot side; demagnetization, magnetic field seeing a decrease at adiabatic process and temperature of MCM decreasing due to MCE; cold blow, fluid flowing from hot side to cold one at isomagnetic process, releasing heat to MCM, and obtaining heat from the heat exchanger at cold end (Petersen et al., 2008; Kitanovski and Egolf, 2006; Bahl et al., 2008; Gómez et al., 2013).

It is true that simulation of numerical models obliged AMR designs. As illustrations, fluid properties showed importance with low fluid flow rate (Ezan et al., 2017), and layered AMR with different MCMs with different Curie temperature was a huge improvement (Aprea et al., 2011; Kamran et al., 2016; Zhang et al., 2017). Furthermore, a review of AMR numerical models was reported, and most of them were one-dimensional (Nielsen et al., 2011).

To intensify the performance of AMR and study temperature distribution in it, a proposed solution of AMR with staggered laminated plates was studied with a 2-dimensional numerical model. Based on the studied model, different parameters were analyzed.

PROPOSED SOLUTION

The proposal was to arrange laminated MCMs staggered in AMR space as if employing breaking segments in layered MCMs. Consequently, the breaking segments of adjacent MCM layers were staggered and broke the regenerator in levels.

This arrangement can reduce thermal conduction from hot to cold ends by increasing the thermal resistance between them due to lower conductivity of working fluid, intensify the heat transfer between MCMs and working fluid radially by broken velocity and thermal boundary layers, and decrease MCM usage.

On the other hand, breaking segments can be arranged to break the boundary layer efficiently. Employing breaking segments instead of decreasing the length of AMR, 0.05L of MCMs at each ends were preserved. Furthermore, breaking boundary layers efficiently indicated that the breaking segments in two adjacent MCM plates should be arranged periodically in axial direction and as far to each other as they could.

Thus, we had the distance of two breaking segments in a level of 0.9L N^{-1}.

In this work, the referenced AMR apparatus was the one of model A built by the research team in University of Ljubliana in Slovenia (Tušek et al., 2013). The outer regenerator dimensions were a length of 80 mm, a width of 39 mm, and a height of 10 mm. AMR of it was composed by 28-layer parallel Gd plates with each thickness of 0.25 mm, distance between two plates of 0.1 mm, total mass of 0.176 kg. Except for total mass of Gd, other parameters were the same for proposed models, and details of them were listed in the Table 1.

Table 1. Centers of breaking segments in axial direction of 7 proposed models. Model A (Tušek et al., 2013) is the referenced model with laminated MCMs. The others are the proposed models with breaking segments. Distribution of breaking segments of model group B, C, and D are regular, near hot side, and near cold side, respectively. Length of a breaking segment of model B1, C1, and D1 are 0.5 mm; the one of B2 and C2 are 1 mm; the one of D3 is 1.5 mm.

Model	A		B1/ B2		C1/ C2		D1/ D2/ D3	
Number of breaking segments in a level	X		8		4		4	
Length of a breaking segment	X		0.5/ 1		0.5/ 1		0.5/ 1/ 1.5	
Distribution of breaking segments	X		Regular distribution		Near hot side		Near cold side	
Numbers of layers	Even	Odd	Even	Odd	Even	Odd	Even	Odd
Numbers of breaking segments	X		8	8	4	4	4	4
Center of breaking segments in axial direction between -40 and 40 (mm)	X		-29.25, -20.25, -11.25, -2.25, 6.75, 15.75, 24.75, 33.75	-33.75, -24.75, -15.75, -6.75, 2.25, 11.25, 20.25, 29.25	6.75, 15.75, 24.75, 33.75	2.25, 11.25, 20.25, 29.25	-29.25, -20.25, -11.25, -2.25	-33.75, -24.75, -15.75, -6.75
Total mass of Gd (kg)	0.1763		0.1675/ 0.1587		0.1719/ 0.1675		0.1719/ 0.1675/ 0.1631	

MODELING OF AMR AND GOVERNING EQUATIONS

The 2-dimensional model of proposed solution can be the final model geometry of a MCM plate and fluid channel. Moreover, to avoid improbable oscillations of fluid temperature at two ends on the interface at fluid velocity approaching zero, two extra channels with length of $H_{channel}$ were employed. Figure 1 illustrates a schematic of the 2-dimensional model of proposed solution. Figure 2 (a) and (b) show the simplification of the full numerical model geometry into repeating units of a referenced model and a proposed model, respectively.

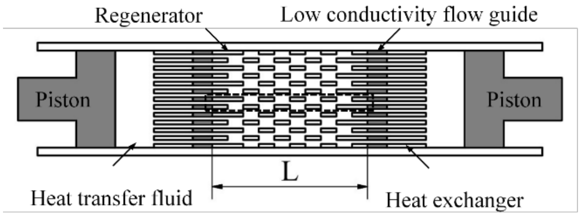

Fig. 1. The full geometry and simulation area of the AMR model.

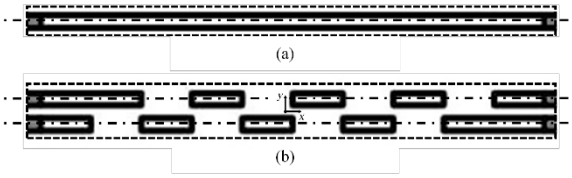

Fig. 2. (a) A repeating unit including half a MCM plate and fluid channel (Model A). (b) A repeating unit including two half MCM plate and a fluid channel (Proposed models).

As a basis of comparison, we had the two-dimensional original model (denoted by model A) with geometry of half a continuous MCM plate and fluid channel with a half thickness of 0.125 mm of MCM and 0.05 mm of fluid channel, a total length of 80 mm of MCM plates, and 28 layers.

According to the assumptions such as isotropic material properties, constant properties of working fluid, no dissipation energy, no slip condition, no chemical reaction and no hysteresis of MCM, the unsteady two-dimensional governing equations for the problem of interest were written as

1. Conservation of mass

$$\frac{\partial}{\partial x_i}(u_i) = 0. \tag{1}$$

2. Conservation of momentum

$$\rho_f \frac{\partial}{\partial t}(u_i) + \rho_f \frac{\partial}{\partial x_i}(u_i u_k) = \mu \frac{\partial}{\partial x_i}\left(\frac{\partial u_k}{\partial x_i}\right) - \frac{\partial p}{\partial x_k}. \tag{2}$$

3. Conservation of energy

$$\rho_f \frac{\partial}{\partial t}\left(C_{P,f} T_f\right) + \rho_f \frac{\partial}{\partial x_i}\left(u T_f\right)_i = k_f \frac{\partial}{\partial x_i}\left(\frac{\partial T_f}{\partial x_i}\right) + a_s h\left(T_{MCM} - T_f\right). \tag{3}$$

$$\rho_{MCM}\frac{\partial}{\partial t}\left(C_{P,MCM}T_{MCM}\right) = k_{MCM}\frac{\partial}{\partial x_i}\left(\frac{\partial T_{MCM}}{\partial x_i}\right) + a_s h\left(T_f - T_{MCM}\right) + \dot{q}_{MCE}. \tag{4}$$

$$\dot{q}_{MCE} = \frac{\rho_{MCM}C_{P,MCM}\Delta T_{ad}}{t_{MCM}}, \tag{5}$$

where $\dot{q}_{MCE}$ was zero at constant magnet field.

Boundary and Initial Conditions

Temperature of exchangers at hot ends and cold ones were 303 and 283 K, respectively. Based on our numerical models and assumptions, the boundary and initial conditions were written below.

1. Symmetry on upper and lower boundary, at $y = \pm\frac{1}{2}\left(H_{channel} + H_{plate}\right)$.

2. Flow

At $x = -\left(\frac{1}{2}L + H_{channel}\right)$,

$$u(t) = \text{fully developed flow with given flow rate.} \tag{6}$$

At $x = \frac{1}{2}L + H_{channel}$,

$$p_{gage} = 0. \tag{7}$$

3. Energy

At $x = -\left(\frac{1}{2}L + H_{channel}\right)$,

$$\begin{cases} T_f = T_L \text{ at } u > 0, \\ \dfrac{\partial T_f}{\partial x} = 0 \; at \; u \leq 0. \end{cases} \tag{8}$$

At $x = \frac{1}{2}L + H_{channel}$,

$$\begin{cases} T_f = T_H \text{ at } u < 0, \\ \dfrac{\partial T_f}{\partial x} = 0 \text{ at } u \geq 0. \end{cases} \tag{9}$$

4. At interface of MCM and working fluid,

$$\begin{cases} \text{No} - \text{slip condition}, \\ u = v = w = 0, \\ h_{convection} = h\left(T_f - T_{MCM}\right). \end{cases} \tag{10}$$

5. Initial conditions

$$\begin{cases} u = v = w = 0, \\ p = 1\;(atm), \\ T_f = T_{MCE} = \dfrac{T_H + T_L}{2} + \dfrac{T_H - T_L}{2}\sin\left(\dfrac{\pi x}{L}\right). \end{cases} \tag{11}$$

Time-Dependent Velocity and Magnetic Field

In this work, average flow rate and magnetic field were periodical functions of time. Figure 3 illustrates the horizontal axis of a non-dimensional time axis in a cycle and the left vertical axis of the magnitude. The flow stagnation time before hot blows (t_1), was set to identical time for stagnation time before cold blows (t_3). Likewise, the hot and cold blow time, t_2 and t_4, respectively, were set to take the same time, which was twice as t_1. Magnetizing/demagnetizing time were equal and took time of t_{MCE}, which was set as 0.1 second. Furthermore, magnetic field remains the same during hot and cold blow time.

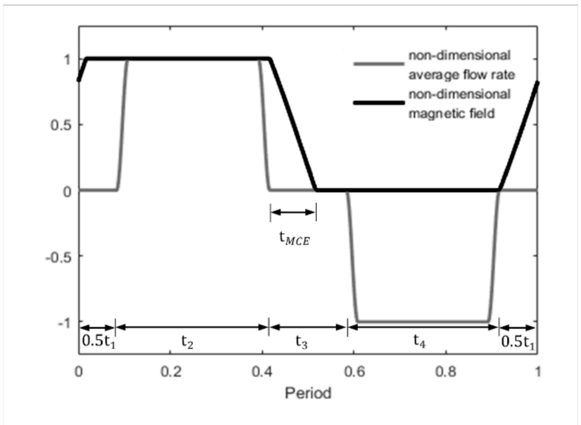

Fig. 3. Non-dimensional average flow rate and magnetic field of an AMR cycle.

The period of 0.6 and 1.2 seconds of an AMR cycle was set; the magnetic field of 0-1 T was employed. Velocity of flows was calculated from average flow rate, which was a function of the utilization factor (ϕ), showed in (12), where $t_{blow} = t_2 = t_4$. Velocity of flow of acceleration and deceleration were sinusoidal function of time, with a total time of 10% of the total flow time. Note that denoted by model A, we employed a fluid channel of 0.05 mm and 28 layers in total.

$$\phi = \frac{\dot{m}C_{p,f}t_{blow}}{m_{MCM}C_{p,MCM}}. \tag{12}$$

However, breaking segments could vary the mass of MCM (m_{MCM}) and change the utilization factor. To compare the performance of AMR, we reduced variation so that the mass flow rate of referenced model was set in proposed models. Set maximum mass flow rates of numerical models were listed in the Table 2.

Table 2. Utilization factor (ϕ) and mass flow rate of referenced model at operation period of 0.6 second.

Utilization factor (ϕ)	0.2	0.4	0.6	0.8
Mass flow rate (kg s^{-1})	0.00967	0.0193	0.0290	0.0387

Material Properties and Mean Field Theory (MFT)

In the work, material properties were referenced based on the research of Petersen et al. (2008), which took Gd as MCM and water as working fluid. Specific heat and adiabatic temperature change of Gd were estimated by MFT at magnetic field change of 0-1 T and variable temperature, density and conductivity were 7900 (kg m^{-3}) and 10.5 (W m^{-1} K^{-1}) evaluated at temperature of 298 K, respectively. Water properties were evaluated at 298 K and listed in the Table 3.

Table 3. Water properties evaluated at 298 K (Petersen et al., 2008).

ρ (kg m^{-3})	C_p (J kg^{-1} K^{-1})	μ (kg m^{-1} s^{-1})	k (W m^{-1} K^{-1})
997	4183	8.91×10^{-4}	0.595

Specific heat and adiabatic change were obtained by self-programming MATLAB (MATLAB 2014a, The MathWorks, Inc.) code in this study.

Heat Convection Coefficient

In this work, flow between parallel plates could be considered. Length of a breaking segment were 0.63-1.88 % of total AMR length so that the flow distribution was affected locally. Hence, the same heat convection coefficient was set in different models.

We employed heat convection coefficient based on the approaching introduced by Nickolay and Martin (2002), and obtained the heat convection coefficient from them as below.

$$h_f = \frac{Nu \cdot k_f}{D_h}. \tag{13}$$

$$Nu = \left[7.541^n + \left(1.841\mathrm{Gz}^{\frac{1}{3}}\right)^n\right]^{\frac{1}{n}}, \quad n = 3.592. \tag{14}$$

The non-dimensional parameters were

$$\mathrm{Gz} = \frac{D_h}{L} RePr, \quad Re = \frac{\rho \bar{V} D_h}{\mu}, \quad Pr = \frac{C_{p,f}\, \mu}{k_f}. \tag{15}$$

where D_h was expressed by the distance between two adjacent plates.

NUMERICAL SOLUTION

Convergence Criteria

To ensure the stability of the numerical solutions of periodical steady state AMR, two convergence criteria of two different cycle lengths were set. The relative differences based on temperature were considered to be convergence criteria with two cycles of adjacency and 100 cycles apart. Where $T(x, y, t)$ represented the temperature at position (x, y) at time t.

$$\begin{cases} max\left(\left|1 - \frac{T(x,y,t-P)}{T(x,y,t)}\right|\right) \le 10^{-6}, \\ max\left(\left|1 - \frac{T(x,y,t-100P)}{T(x,y,t)}\right|\right) \le 10^{-4}. \end{cases} \tag{16}$$

Performance Evaluation of AMR

There were four criteria to judge the performance of an AMR; two were the cooling and heating power of an apparatus, (17) and (18) respectively; the others were specific cooling and heating power based on mass of used MCM, (19) and (20) respectively. On the one hand, cooling and heating power showed the refrigeration ability and requirement to heat exchanger at room temperature side. Note that compared with the complete MCM plates, proposed solution employed MCM with lower mass.

$$\dot{Q}_c = \frac{1}{period} \int_0^{t_{cold\ blow}} \dot{m}\, C_{p,f}\left[T_L - T_f(t)\right] dt. \tag{17}$$

$$\dot{Q}_h = \frac{1}{period} \int_0^{t_{hot\ blow}} \dot{m}\, C_{p,f}\left[T_f(t) - T_H\right] dt. \tag{18}$$

$$\dot{q}_c = \frac{\dot{Q}_c}{m_{MCM}}. \tag{19}$$

$$\dot{q}_h = \frac{\dot{Q}_h}{m_{MCM}}. \tag{20}$$

Note that with a time step of 2.5×10^{-3} second, relative temperature differences between two adjacent cycles could reach an order of 10^{-7} and 10^{-10} at a period of 0.6 second at $\varphi \leqq 0.4$ and $\varphi \geqq 0.6$, respectively. Moreover, relative difference of cooling/heating power could be less than 0.1% when relative temperature differences between two adjacent cycles reached an order of 10^{-7}.

SOFTWARE PACKAGE SETTINGS

A 2-dimensional model was created and “Heat Transfer in Soilds, Heat Transfer in Fluids, and Laminar flow” of COMSOL Multiphysics software package (Comsol Inc., version 5.4) were employed.

Functions of velocity and magnetic field, MCE function of local MCM temperature and magnetic field, convective heat transfer coefficient function of average velocity due to fixed geographical parameters, and relative temperature differences between two adjacent cycles and 100-cycle-apart cycles were built.

According to the grid independent test, we had mesh size listed in Table 4, time step of 2.5×10^{-3} second, “Relative error” of 10^{-3} to 10^{-4}, and “Absolute tolerance” of 10^{-8} were employed.

Table 4. Details of meshes.

Maximum element size (m)	Minimum element size (m)	Maximum element growth rate	Curvature factor	Resolution of narrow regions
1.03×10^{-5}	1.19×10^{-7}	1.08	0.25	1

RESULTS AND DISCUSSION

Cooling/Heating Power of Model A (Referenced Model)

Figure 4 illustrates the cooling and heating powers as a function of utilization factor at operation period of 0.6 and 1.2 seconds. According to this figure, the range of cooling power is around between 60 and 95 W respectively. The heating powers reach peaks of slightly less than 130 and 120 W at utilization factor of 0.4 and 0.8, respectively. To provide a stronger cooling power, referenced model prefers to the longer operation period between 0.6 and 1.2 second, which means with an operation period of 0.6 second and same utilization factor, the flow rate is too great for working fluid to acquire whole cooling and heating power from the regenerator. Thus, the greater heat transfer in the radial direction can release more of the remaining freezing power in the AMR for the operation period of 0.6 second.

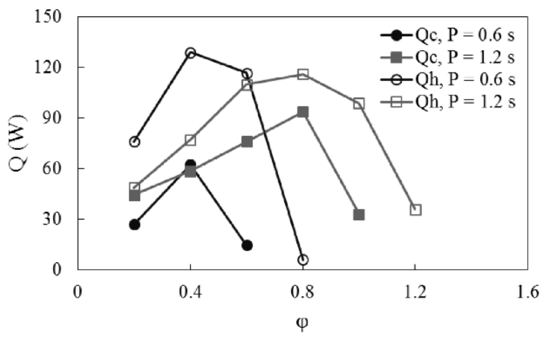

Fig. 4. Cooling and heating powers of model A as functions of utilization factor at operation periods of 0.6 and 1.2 seconds.

For a working refrigeration system, the heating requirement should be larger than cooling power (Qh > Qc) with defined positive Qh and Qc. It is better that the difference between cooling and heating power of an AMR system is smaller. The large difference between cooling and heating power hinders the potential of commercialization due to larger difference between flow rate requirement at hot and cold blow time. Furthermore, a greater difference between the cooling power and the heat dissipation power means that both the local cooling power and heat dissipation still remain in the AMR. At the fixed temperature on both sides, a large difference between cooling and heating power signifies large local difference of temperature distribution in AMR between just before magnetizing and demagnetizing due to the variation of MCM specific heat and adiabatic temperature distribution.

The difference between cooling and heating power represents the net heating power from MCE. According to the definitions of cooling and heating power and zero change of total energy in a periodically steady cycle, the difference between cooling and heating power (Q_h-Q_c), which is the net heating source from MCE, is not only the power input of an AMR, but also the equivalent MCE difference between magnetizing and demagnetizing in the AMR system.

Cooling/Heating Power of Proposed Solution

A comparison of AMR geometries including the referenced model was investigated by Tušek et al. (2013). With 2D numerical models, this work further studied the performance of the proposed models with the novel design of staggered breaking segments in rectangular MCM plates.

Figures 5-7 show the cooling and heating powers versus the flow rate for different models. The performance of model C1 is the best among models A, B and C (Figures 5 and 7). Similarly, the performance of model D2 is the best among models A and D (Figure 7). Therefore, the models C1 and D2 are our potential models.

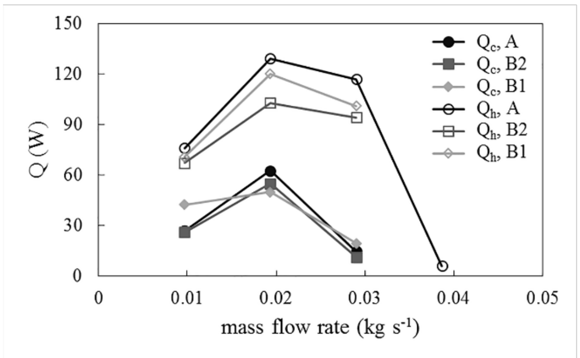

Fig. 5. Cooling and heating powers of models A, B1 and B2 as functions of mass flow rate at the operation period of 0.6 second.

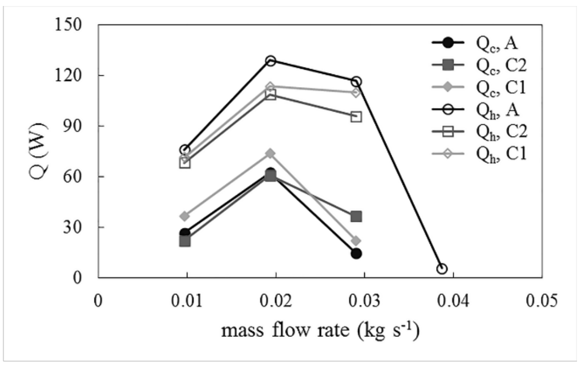

Fig. 6. Cooling and heating power of model A, C1 and C2 as functions of mass flow rate at the operation period of 0.6 second.

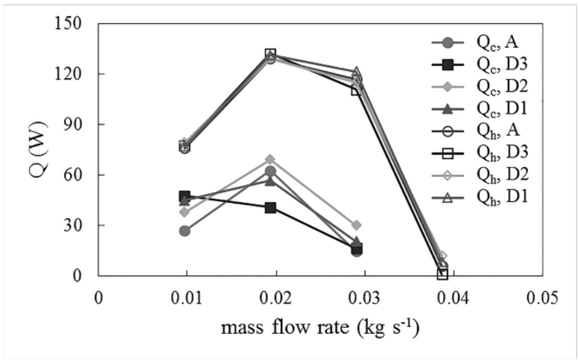

Fig. 7. Cooling and heating power of model A, D1, D2 and D3 as functions of mass flow rate at the operation period of 0.6 second.

As the cooling capacity increases with an increase in flow rate, the difference of cooling capacities between the two potential models is less than 5%. Figure 8 illustrates the cooling and heating powers as a function of mass flow rate for models A (referenced model), C1 and D2. The models A, C1, and D2 reach peaks of around 62, 69, and 73 W at mass flow rate of 0.019 kg s^{-1}, respectively. Moreover, models C1 and D2 provide the cooling power of approximate 37 W with a small difference of 0.2 W at mass flow rate of 0.0097 kg s^{-1}.

On the other hand, the model C1 is the best choice to minimize the working load of heat exchangers. As shown in Figure 8, the heating power of model C1 model reaches a peak of approximate 113 W, which is around 6 W lower than the others for the mass flow rate of 0.029 kg s^{-1}.

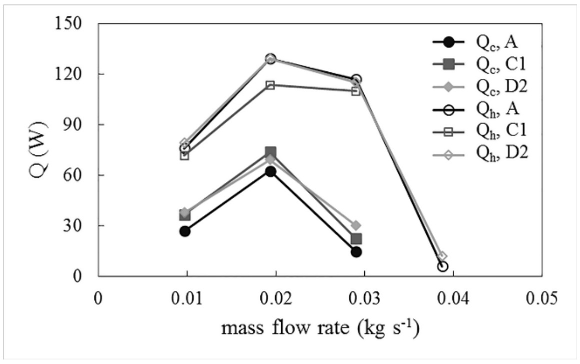

Fig. 8. Cooling and heating power of model A, C1 and D2 as functions of mass flow rate at the operation period of 0.6 second.

Furthermore, the difference of utilization factors at fixed mass flow rate for different models is caused by MCM mass, which has a maximum difference of only 5 %. Figure 9 illustrates the cooling and heating powers per mass of MCM (specific power) as a function of mass flow rate, respectively. Likewise, the model C1 shows the greatest specific cooling power and smallest specific heating power at the mass flow rate of 0.019 kg s^{-1} among models A, C1 and D2.

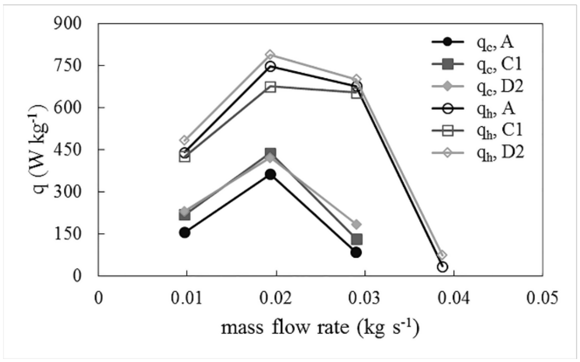

Fig. 9. Specific cooling and heating powers of model A, C1 and D2 as a function of mass flow rate at the operation period of 0.6 second.

Comparison of T(x) between Potential Models

For models A, C1 and D2, the mass flow rate of 0.019 kg s^{-1} is deficient to release heating power from regenerators. From a viewpoint of an optimal AMR, the average temperature of working fluid at hot side should be equal to the one of hot-side heat exchanger. With boundary layers included in this study, Figure 10 shows that the central line temperature of working fluid at the hot end is about 303.3 K for three models.

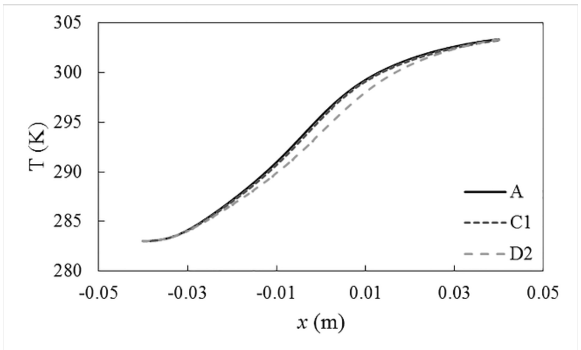

Fig. 10. Axial temperature distribution along center lines of working fluid for models A, C1, and D2 just after hot blow time at the mass flow rate of 0.019 kg s^{-1}.

On the other hand, for three models, mass flow rate of 0.019 kg s^{-1} is deficient for heating power but may be excessive for cooling power. This fact implies that these three models are not optimal AMRs at the same flow rate for hot and cold blows. Figures 10 and 11 show that all three models obtain temperature of about 283.4 and 303.6 K with a small temperature difference of 0.1 K on the cold and hot sides just after cold and hot blows, respectively. This result means that smaller cold-blow and larger hot-blow flow rate are needed to optimize the performance, and none of these three AMR models are optimal one.

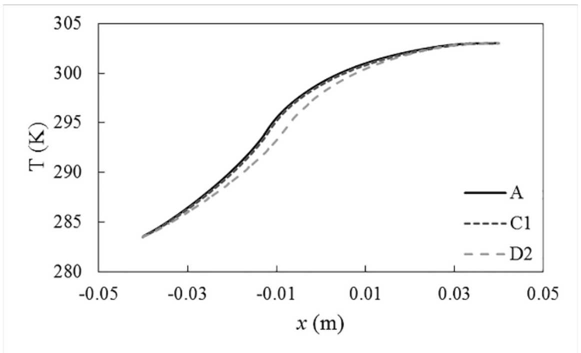

Fig. 11. Axial temperature distribution along center lines of working fluid for models A, C1, and D2 just after cold blow time at the mass flow rate of 0.019 kg s^{-1}.

Pressure Drops between Two Ends of AMRs

Breaking segments bring not only less MCM usage and secondary flow to AMR but also lower pump requirement. Table 5 shows pressure drops at maximum flow rate in AMRs. Compared to model A, models C1 and D2 obtain lower pressure drops around 4% and 8% between two ends, respectively.

Table 5. Pressure drops at maximum flow rate in AMRs.

Mass flow rate (kg s^{-1})	Names of the models		
	Model A (kPa)	Model C1 (kPa)	Model D2 (kPa)
0.0097	7.63	7.36	6.99
0.019	15.27	14.81	14.02
0.029	22.90	22.23	21.12
0.039	30.53	29.72	28.28

CONCLUSIONS

The efficiency of AMR refrigeration systems with staggered laminated plates is investigated by 2D numerical models in this work. The main idea of the novel design is to reduce heat conduction from hot to cold ends and break the boundary layers by secondary flow.

Performance of an AMR can be intensified by breaking segments with a proper length at different distributions. Compared to the referenced model, model B1 provides a greater cooling power at mass flow rates of 0.0097 and 0.029 kg s^{-1}, but a smaller cooling power at mass flow rate of 0.019 kg s^{-1} at operation period of 0.6s. Model C1 and D2 are able to provide greater cooling power. Furthermore, model C1 reduces the heating power, which represents the requirement of the heat exchangers at the hot side. For 4 breaking segment in a level in the distribution of near hot and cold side, the length of them of 1 mm and 1.5 mm are too long to optimize the referenced AMR model.

Among the numerical models in the study, model C1 shows the best performance. Compared to the referenced model, C1 model decreases the usage of MCM by 2.5%, increases the cooling power from 62.5 to 69.1 watts, and reduces the heating power from 129.1 to 113.4 watts, as well as the pressure drops between two ends of the AMR around 4% at the magnetic field changes of 0-1 T, the temperature of the hot to cold ends of 283-303 K, the operation period of 0.6 seconds, and the utilization factor of about 0.4.

This study illustrates that the novel design of AMR with staggered laminated plates can improve the performance of an AMR refrigeration system.

ACKNOWLEDGEMENT

This work is funded by the Ministry of Science and Technology in Taiwan under contract of MOST 108-2221-E-007-103.

REFERENCES

Aprea, C., Greco, A., and Maiorino, A., “A numerical analysis of an active magnetic regenerative cascade system,” International Journal of Energy Research, 35(3), 177-188 (2011).

Bahl, C. R. H., Petersen, T. F., Pryds, N., and Smith, A., “A versatile magnetic refrigeration test device,” Review of Scientific Instruments, 79(9), 093906 (2008).

Balli, M., Fruchart, D., and Gignoux, D., “Optimization of La (Fe, Co) 13− xSix based compounds for magnetic refrigeration,” Journal of Physics: Condensed Matter, 19(23), 236230 (2007).

Balli, M., Jandl, S., Fournier, P., and Kedous-Lebouc, A., “Advanced materials for magnetic cooling: Fundamentals and practical aspects,” Applied Physics Reviews, 4(2), 021305 (2017).

Chen, Y. F., Wang, F., Shen, B. G., Hu, F. X., Sun, J. R., Wang, G. J., and Cheng, Z. H., “Magnetic properties and magnetic entropy change of LaFe11. 5Si1. 5Hy interstitial compounds,” Journal of Physics: Condensed Matter, 15(7), L161 (2003).

Ezan, M. A., Ekren, O., Metin, C., Yilanci, A., Biyik, E., and Kara, S. M., “Numerical analysis of a near-room-temperature magnetic cooling system,” International Journal of Refrigeration, 75, 262-275 (2017).

Franco, V., Blázquez, J. S., Ingale, B., and Conde, A., “The magnetocaloric effect and magnetic refrigeration near room temperature: materials and models,” Annual Review of Materials Research, 42 (2012).

Gómez, J. R., Garcia, R. F., Catoira, A. D. M., and Gómez, M. R., “Magnetocaloric effect: A review of the thermodynamic cycles in magnetic refrigeration,” Renewable and Sustainable Energy Reviews, 17, 74-82 (2013).

Gschneidner Jr, K. A. and Pecharsky, V. K., “Thirty years of near room temperature magnetic cooling: Where we are today and future prospects," International Journal of Refrigeration, 31(6), 945-961 (2008).

Gschneidner Jr, K. A., Pecharsky, V. K., and Tsokol, A. O., "Recent developments in magnetocaloric materials," Reports on progress in physics, 68(6), 1479 (2005).

Kamran, M. S., Ali, H., Farhan, M., Tang, Y. B., Chen, Y. G., and Wang, H. S., "Performance optimisation of room temperature magnetic refrigerator with layered/multi-material microchannel regenerators," International Journal of Refrigeration, 68, 94-106 (2016).

Kitanovski, A., and Egolf, P. W., "Thermodynamics of magnetic refrigeration," International Journal of Refrigeration, 29(1), 3-21 (2006).

Kitanovski, A., Plaznik, U., Tušek, J., and Poredoš, A., "New thermodynamic cycles for magnetic refrigeration," International Journal of Refrigeration, 37, 28-35 (2014).

Klinar, K., Tomc, U., Jelenc, B., Nosan, S., and Kitanovski, A., "New frontiers in magnetic refrigeration with high oscillation energy-efficient electromagnets," Applied energy, 236, 1062-1077 (2019).

Lee, S. J., Kenkel, J. M., Pecharsky, V. K., and Jiles, D. C., "Permanent magnet array for the magnetic refrigerator," Journal of Applied Physics, 91(10), 8894-8896 (2002).

Liu, J., Gottschall, T., Skokov, K. P., Moore, J. D., and Gutfleisch, O., "Giant magnetocaloric effect driven by structural transitions," Nature materials, 11(7), 620-626 (2012).

Mahdy, A. M. J., "Overview for published Magnetocaloric Materials used in Magnetic Refrigeration applications," International Journal of Computation and Applied Sciences, 3, 192-200 (2017).

Nickolay, M., and Martin, H., "Improved approximation for the Nusselt number for hydrodynamically developed laminar flow between parallel plates," International journal of heat and mass transfer, 45(15), 3263-3266 (2002).

Nielsen, K. K., Tusek, J., Engelbrecht, K., Schopfer, S., Kitanovski, A., Bahl, C. R. H., Smith, A., Pryds, N., and Poredos, A., "Review on numerical modeling of active magnetic regenerators for room temperature applications," International Journal of Refrigeration, 34(3), 603-616 (2011).

Petersen, T. F., Pryds, N., Smith, A., Hattel, J., Schmidt, H., and Knudsen, H. J. H., "Two-dimensional mathematical model of a reciprocating room-temperature active magnetic regenerator," International Journal of Refrigeration, 31(3), 432-443 (2008).

Raich, H., and Blümler, P., "Design and construction of a dipolar Halbach array with a homogeneous field from identical bar magnets: NMR Mandhalas," Concepts in Magnetic Resonance Part B: Magnetic Resonance Engineering: An Educational Journal, 23(1), 16-25 (2004).

Shah, H. V., Shahapure, R. M., Menghani, P.D., and Sawant, V. P., "Study of Magnetic Refrigerator Based on AMR Cycle," International Conference on Ideas, Impact and Innovation in Mechanical Engineering ICIIIME 5: 582–588 (2017).

Tušek, J., Kitanovski, A., Zupan, S., Prebil, I., and Poredoš, A., "A comprehensive experimental analysis of gadolinium active magnetic regenerators," Applied Thermal Engineering, 53(1), 57-66 (2013).

Tušek, J., Zupan, S., Prebil, I., and Poredoš, A., "Magnetic cooling-development of magnetic refrigerator," Strojniški vestnik, 5(55), 293-302 (2009).

Yu, B. F., Gao, Q., Zhang, B., Meng, X. Z., and Chen, Z., "Review on research of room temperature magnetic refrigeration," International Journal of Refrigeration, 26(6), 622-636 (2003).

Yu, B., Liu, M., Egolf, P. W., and Kitanovski, A., "A review of magnetic refrigerator and heat pump prototypes built before the year 2010," International Journal of Refrigeration, 33(6), 1029-1060 (2010).

Zhang, M., Abdelaziz, O., Momen, A. M., and Abu-Heiba, A., "A numerical analysis of a magnetocaloric refrigerator with a 16-layer regenerator," Scientific reports, 7(1), 1-12 (2017).

交錯層狀磁製冷再生器之效能提升設計

張哲維　　許文震

國立清華大學動力機械工程學系

摘 要

磁製冷再生系統不需壓縮機與冷媒即可製冷，是一極有潛力的冷凍技術。然兩熱傳現象為目前的效能瓶頸：一為磁熱材料與工作流體間的熱傳速度；二為由熱端至冷端的熱量傳遞。

本研究於平板式磁製冷再生器中增加交錯斷點，透過數值模擬比較 80 mm 長的再生器設計。與原再生器相比，C1 模型能減少 2.5% 之磁熱材料使用；在 0-1 特斯拉、283-303K 的溫差、工作週期 0.6 秒、利用因數約 0.4 時，將冷凍力由 62.48 增至 69.10 瓦。本研究證實，透過交錯層狀磁製冷再生器之設計，能增加磁製冷裝置之效能。